

Mechanochemical Synthesis of Bumetanide–4-Aminobenzoic Acid Molecular Cocrystals: A Facile and Green Approach to Drug Optimization

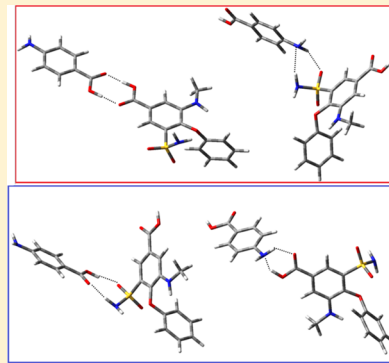
Giovanna Bruni,^{*,†} Mariarosa Maietta,[†] Vittorio Berbenni,[†] Piercarlo Mustarelli,[†] Chiara Ferrara,[†] Mauro Freccero,[‡] Vincenzo Grande,[‡] Lauretta Maggi,[§] Chiara Milanese,[†] Alessandro Girella,[†] and Amedeo Marini[†]

[†]C.S.G.I. - Department of Chemistry, Physical-Chemistry Section, University of Pavia, Viale Taramelli 16, 27100 Pavia, Italy

[‡]Department of Chemistry, Organic Chemistry Section, University of Pavia, Viale Taramelli 10, 27100 Pavia, Italy

[§]Department of Drug Sciences, University of Pavia, Viale Taramelli 12, 27100 Pavia, Italy

ABSTRACT: Molecular cocrystals are of growing interest in pharmaceuticals for their improved physicochemical properties. Their mechanochemical synthesis is very promising, being easy, cheap, and “green”. Here, for the first time, we report on cocrystallization of bumetanide, a diuretic and natriuretic active principle, and 4-aminobenzoic acid. The synthesis is performed both by wet and dry grinding. The cocrystal formation was investigated with a wide range of techniques, including solid-state NMR, IR, XRD, microscopy, and thermal analysis. Wet and dry grinding procedures led to different cocrystal polymorphs. In particular, the dry method gave a cocrystal by powder amorphization and subsequent crystallization. DFT calculations at the B3LYP/6-31+G(d,p) level of theory shed light on the H-bond scheme at the basis of cocrystal formation. The cocrystals showed improved solubility and dissolution rate with respect to the drug alone. This could guarantee a faster absorption and a better bioavailability of the active principle.



1. INTRODUCTION

Co-crystal synthesis is a modern and powerful approach able to improve the solid-state properties of a drug, and particularly its solubility and bioavailability.^{1,2} Recently, the US FDA published a document where appropriate classification of cocrystals and the regulatory implications of this classification are treated, thus paving the way for their use in new chemical entities and generic products.³ A wide range of techniques to prepare these crystalline materials were reported in the literature, including solvent evaporation, sublimation, growth from the melt, slurries, solid state grinding, kneading, and several other methods like antisolvent addition, supercritical fluid, and ultrasound-assisted processing.^{4–7} Recently, the strong and increasing demand for clean and environmentally friendly processes has focused the attention on “green methods” such as dry and wet grinding, also known as kneading.⁸ The increasing success of mechanochemistry in the synthesis of pharmaceutical cocrystals is due to the fact that supramolecular interactions responsible for cocrystal formation (hydrogen bonds, halogen bonds, $\pi-\pi$ stacking interactions) can be broken and reformed under mild mechanical agitation. The addition of a small amount of solvent during grinding can further accelerate mechanochemical reactions between solids, thus promoting cocrystal formation. Thus, kneading combines the synthetic advantages of mechanochemistry (simplicity and lack of bulk solvent) with fast reaction rates, high yields, and product

crystallinity. These advantageous properties made kneading a method of choice for cocrystal formation.^{8–11}

Bumetanide (3-*n*-butylamino-4-phenoxy-5-sulfamoyl-benzoic acid) (Scheme 1a) is a potent diuretic drug used in the treatment of edema associated with congestive heart failure and hepatic and renal diseases and to cure mild or moderate hypertension. Its principal site of action is the thick ascending limb of the Henle loop, where it exerts its diuretic and natriuretic effect.^{12,13} It produces a rapid and marked diuresis, thus increasing urinary excretion of sodium, chloride, and other electrolytes which persists for several hours. However, a low water solubility restricts its oral bioavailability and limits its use to low-volume parenteral formulations.¹⁴ The use of salts is a common strategy to enhance the solubility of acidic and basic drugs, and the formation of sodium and potassium salts of bumetanide trihydrate has been described in the literature.^{15,16}

In this paper, we faced the low solubility problem of bumetanide by investigating cocrystal formation. We prepared bumetanide cocrystals by both dry and wet grinding. To this aim, we selected a number of coformers (most of them carboxylic acids) possessing functional groups which are able to generate H-bond motifs with the drug (in particular with the

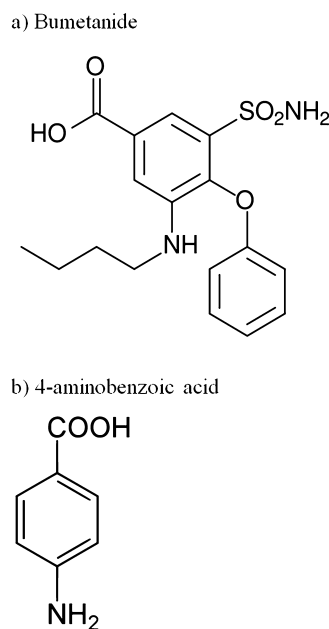
Received: April 2, 2014

Revised: June 23, 2014

Published: July 18, 2014



Scheme 1. Chemical Structures of Bumetanide (a) and 4-Aminobenzoic Acid (b)



carboxylic acid group, the sulfur and the amino group of the bumetanide molecule). We obtained the formation of cocrystals only using 4-aminobenzoic acid (Scheme 1b) as the coformer. The 4-aminobenzoic acid, in the quantity used, is comprised in the Generally Recognized as Safe (GRAS) list of the FDA. Co-crystal formation was investigated by means of thermogravimetric analysis (TGA), differential scanning calorimetry (DSC), X-ray powder diffraction (XRPD), Fourier infrared spectroscopy (FT-IR), solid-state NMR (SSNMR), and scanning electron microscopy coupled with energy dispersive X-ray spectrometry (SEM-EDS).^{17–19} The solubility and dissolution rate of the binary systems were investigated, to establish if the cocrystallization process caused an enhancement of these parameters compared to pure bumetanide.

2. EXPERIMENTAL PROCEDURES

2.1. Materials. Bumetanide (*B*) was kindly donated by Fidia Farmaceutici S.p.A. (Abano Terme PD, Italy), and the coformers were obtained from Sigma-Aldrich Company (Milan, Italy). Among the selected coformers (succinic acid, sorbic acid, glutaric acid, fumaric acid, salicylic acid, L-tartaric acid, sorbitol, mannitol, saccharine, *p*-benzoquinone), only 4-aminobenzoic acid (*AB*) gave interesting results that will be reported in this paper.

The binary systems were prepared using two different grinding methods:

- Kneading: The drug and the coformer (both in powder) were mixed in 1:1 molar ratio and manually ground in an agate mortar for 1 h, adding few drops of ethanol. The sample will be named *BAB1:1kn* in the following.
- Dry grinding: The components in 1:1 molar ratio were ground in a planetary mill (Pulverisette 7, Fritsch, Germany) at a rate of 500 rpm with 50 agate balls (5 mm diameter, weight of each ball: about 175 mg) for different times. The ground samples will be coded as *BAB1:1mp* followed by the time of grinding (*BAB1:1mp15min*, *BAB1:1mp30min*, etc.).

2.2. Characterizations. **2.2.1. Thermal Analysis.** The thermal behavior of the samples was characterized using TGA Q2000 IR and DSC Q2000 instruments, both interfaced with a TA 5000 data station (TA Instruments, NewCastle, DE, USA). The DSC instrument was calibrated using ultrapure (99.999%) indium (melting point = 156.6 °C; $\Delta H = 28.54 \text{ J g}^{-1}$) as a standard. Samples (3–5 mg) were placed in open standard aluminum pans under a continuously purged N₂ atmosphere (flow rate 45 mL·min⁻¹), and heating was carried out at 10 K·min⁻¹. All data from thermal measurements are the average of three or more experiments.

2.2.2. Spectroscopic Techniques. FT-IR spectra were recorded on a Nicolet FT-IR iS10 Spectrometer (Nicolet, Madison, WI, USA). Data were collected in ATR (attenuated total reflectance) mode (Smart iTR with ZnSe plate) by coadding 256 scans in the 4000–650 cm⁻¹ range with a resolution of 4 cm⁻¹.

2.2.3. X-ray Powder Diffraction. X-ray powder diffractograms were collected on a D5005 Bruker diffractometer (Karlsruhe, Germany) using Cu K α radiation ($\lambda(\text{K}\alpha_1) = 1.54056 \text{ \AA}$) equipped with a θ - θ vertical goniometer, Ni filter, monochromator, and scintillator counter. The patterns were recorded at room temperature in step scan mode (step size, 0.020°; counting time, 3 s per step) in the 2 θ angular range 5–35° (accelerating voltage of 40 kV and current of 40 mA).

2.2.4. Microscopic Analysis. SEM measurements and energy dispersive microanalysis were performed using a Zeiss EVO MA10 (Carl Zeiss, Oberkochen, Germany) coupled with an EDS detector (X-max 50 mm², Oxford Instruments, Oxford, U.K.).

2.2.5. Solid-State NMR. Solid-state NMR spectra were acquired with a 400 MHz spectrometer (Avance III, Bruker, Karlsruhe, Germany) based on a wide-bore 9.4 T magnet equipped with a 4 mm MAS probe. ¹³C spectra were acquired with ¹H–¹³C CPMAS. The ¹H 90° pulse was 4 μ s, the delay time 30 s, and the contact time 2 ms, and the signals were averaged over 8k acquisitions for CP. The rotation frequency was 11 kHz for ¹H and 11 kHz for ¹³C. Signal chemical shifts were referenced to TMS. The spectra were processed and analyzed with the package TOPSPIN (Bruker).

2.2.6. Solubility and Dissolution Rate. The solubility was determined in triplicate, in distilled water, at 21 °C, by pouring an excess of bumetanide or of the new phases, in volumetric flasks. The flasks were left under magnetic stirring at 300 rpm,

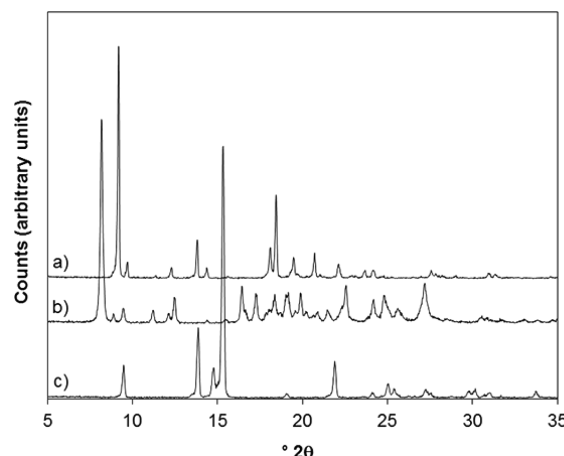


Figure 1. XRPD patterns of (a) bumetanide, (b) *BAB1:1kn*, and (c) 4-aminobenzoic acid.

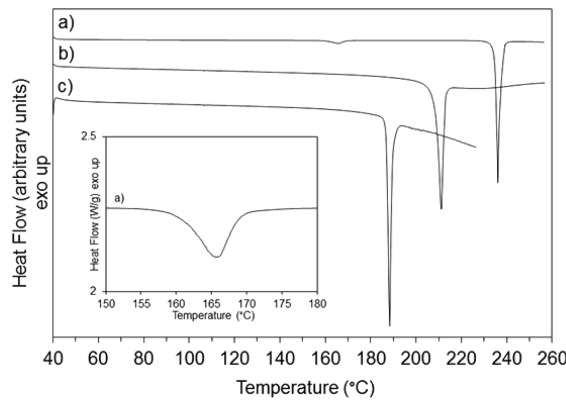


Figure 2. DSC curves of (a) bumetanide, (b) *BAB1:1kn*, and (c) 4-aminobenzoic acid. In the inset, the enlarged view of the transition peak of bumetanide is shown.

and the concentration was determined at different time intervals until equilibrium was reached. The suspension was

filtered ($0.22\text{ }\mu\text{m}$, Millipore) and properly diluted. The absorbance was determined with a UV-visible double beam spectrophotometer (Lambda 25 UV Winlab V6 software, PerkinElmer, Monza, Italy) at 220 nm for bumetanide and also at 265 nm for 4-aminobenzoic acid, in the case of the new products.

3. RESULTS AND DISCUSSION

3.1. The Wet Grinding (Kneading) Product. As evident in Figure 1, the XRPD pattern of the sample *BAB1:1kn* (curve b) is significantly different from those of the pure components (curves a and c), thus indicating that the product obtained by kneading is a new crystalline phase. The TG analysis (not shown) also demonstrates that the sample is free of solvent.

In Figure 2, the DSC curve of the sample *BAB1:1kn* is compared to those of bumetanide and coformer. As described in the literature,^{20,21} at $160.6 \pm 0.7\text{ }^\circ\text{C}$, pure bumetanide shows the transition ($\Delta H = 4.2 \pm 0.3\text{ J/g}$) from polymorph II to polymorph I (see inset in Figure 2), followed by a sharp

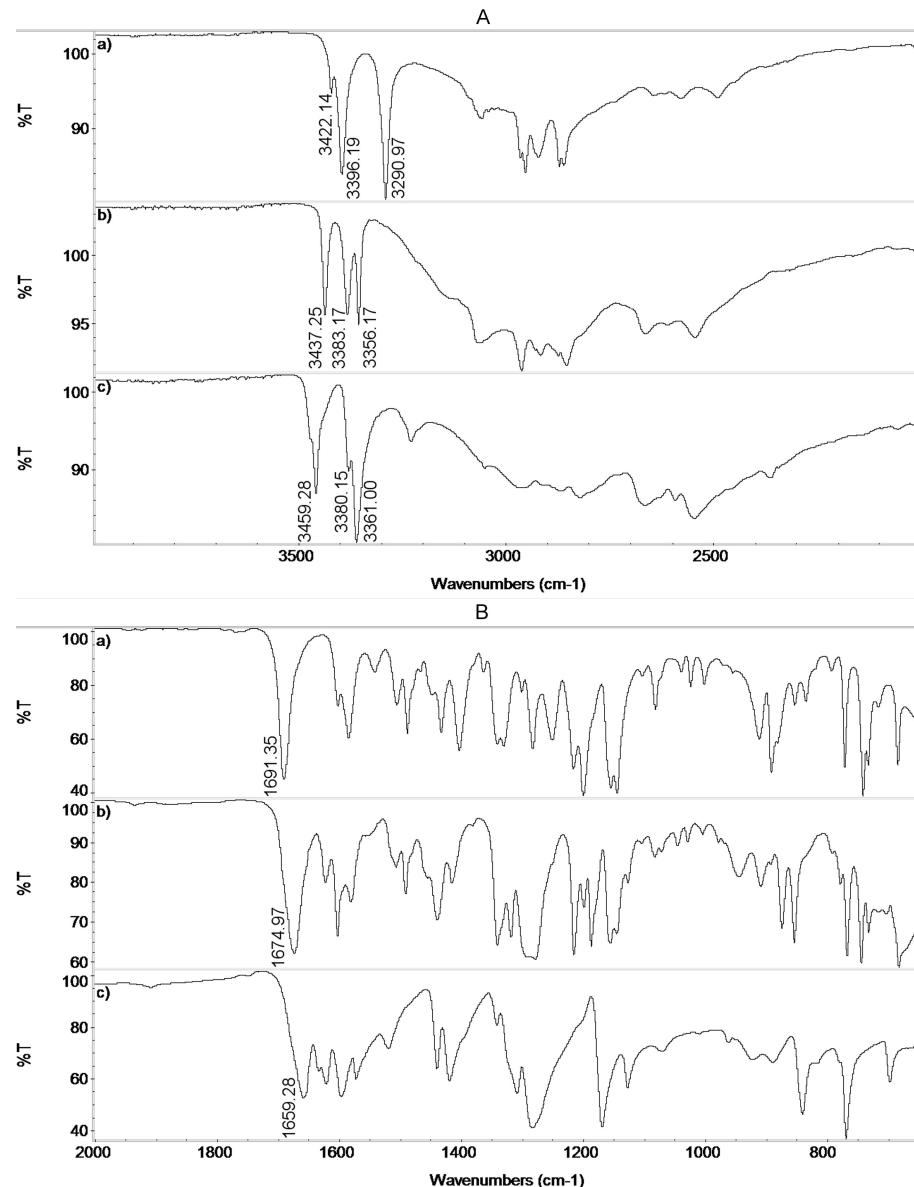


Figure 3. FT-IR spectra of (a) bumetanide, (b) *BAB1:1kn*, and (c) 4-aminobenzoic acid in the frequency region $4000\text{--}2000\text{ cm}^{-1}$ (A) and $2000\text{--}650\text{ cm}^{-1}$ (B).

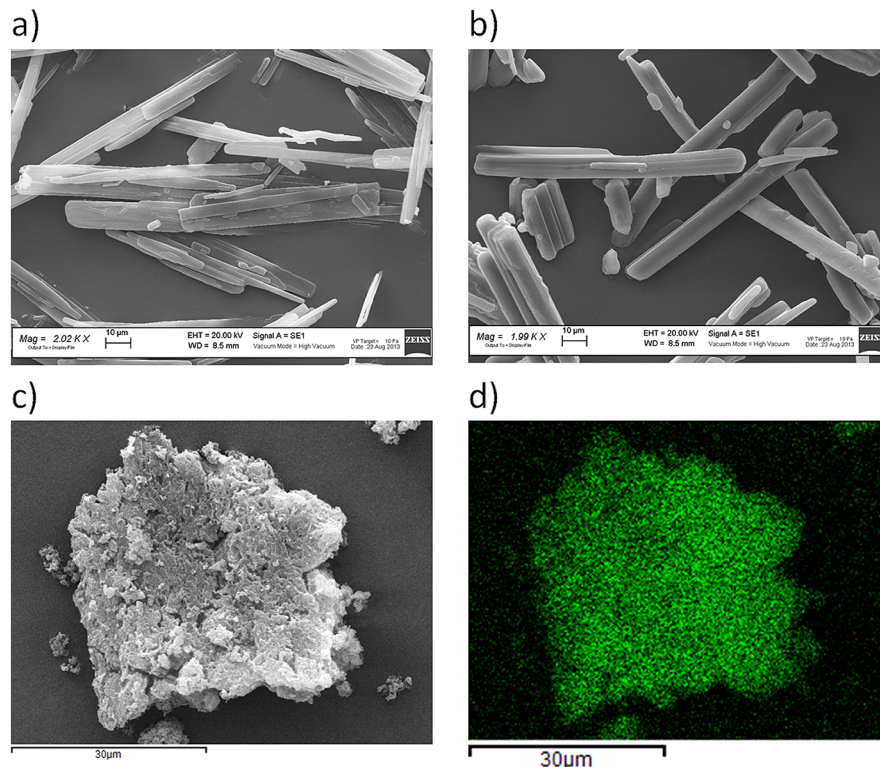


Figure 4. Microphotographs of (a) bumetanide, (b) 4-aminobenzoic acid, and (c) BAB1:1kn and (d) a sulfur map of BAB1:1kn.

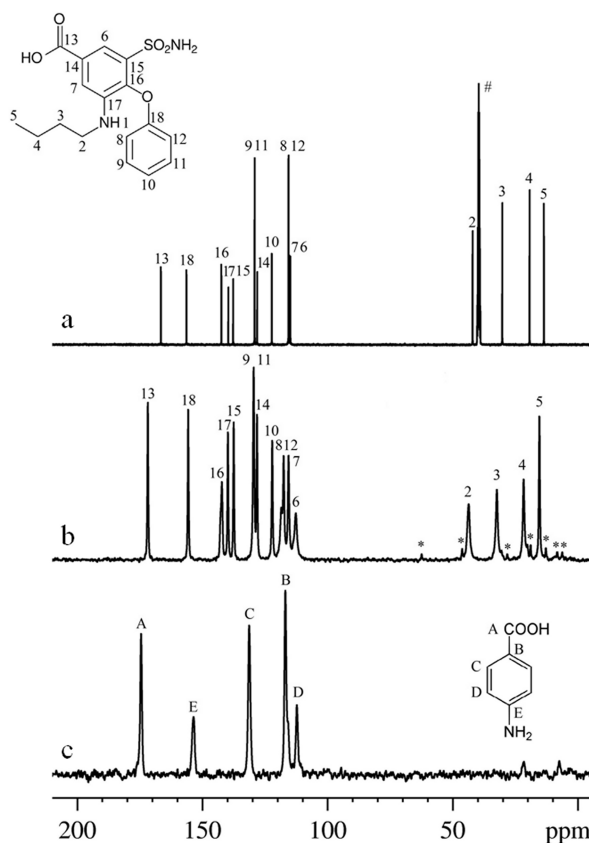


Figure 5. ^{1}H - ^{13}C CPMAS NMR spectra of (a) bumetanide in solution, (b) bumetanide polycrystalline sample, and (c) 4-aminobenzoic acid. #, solvent signals; *, spinning sidebands.

endothermic peak at 234.3 ± 0.6 °C ($\Delta H = 125.1 \pm 1.6$ J/g) due to the melting of form I. The coformer AB (Figure 1,

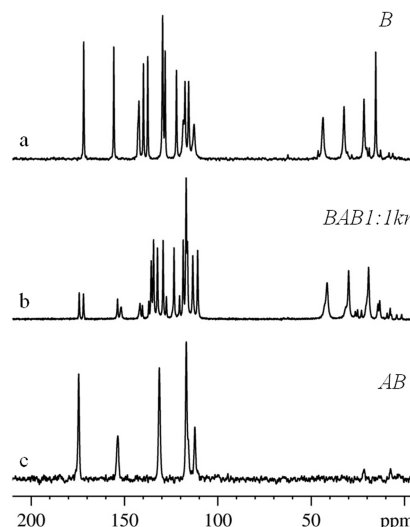


Figure 6. ^{1}H - ^{13}C CPMAS NMR spectra of (a) bumetanide polycrystalline sample, (b) BAB1:1kn cocrystal, and (c) 4-aminobenzoic acid.

curve c) melts at 187.5 ± 0.6 °C with an enthalpy change of 162.7 ± 1.0 J/g.

In the DSC trace of the BAB1:1kn sample (Figure 1, curve b), a sharp endothermic peak at 209.6 ± 1.0 °C with an enthalpy change of 138.7 ± 0.4 J/g appears, and no traces of the thermal events of pure components are evident. The new peak falls between the melting temperatures of bumetanide (234.3 °C) and 4-aminobenzoic acid (187.5 °C). This behavior clearly proves that during kneading a new solid phase has been formed, in agreement with the XRPD results.²²

FT-IR spectra have been acquired in order to confirm the coformer formation and to gain knowledge about the functional

groups involved in the interactions between the two starting molecules. Indeed, spectral changes in cocrystals with respect to the pure components are expected as a consequence of the synthon formation. As the hydrogen bond is one of the most important interactions at the basis of the formation of supramolecular synthons, FT-IR analysis is considered a powerful tool for this kind of investigation. In Figure 3, it is evident that the spectrum of the sample *BAB1:1kn* is not the simple sum of the components spectra, but several significant differences are present. The main changes concern the absorptions of the sulfonamide N—H stretching of bumetanide (asymmetric at 3396 cm^{-1} and symmetric at 3291 cm^{-1} in pure bumetanide), the asymmetric and symmetric stretching of the amino group of the pure coformer (at 3459 and 3361 cm^{-1} , respectively), and the carboxylic C=O stretching of both components (at 1691 cm^{-1} for bumetanide and 1659 cm^{-1} for 4-aminobenzoic acid). The changes of these vibrational frequencies prove that the above-mentioned functional groups of the two components do participate in a new hydrogen bond network, thus identifying the cocrystal formation.

The morphologies of the pure drug and coformer particles are very similar, with both of them being in the shape of smooth rods a few dozen micrometers long (Figure 4a,b). The *BAB1:1kn* sample is made of aggregates of smaller particles nearly melted together (Figure 4c). We have performed the elemental microanalysis on *BAB1:1kn* recording the map of sulfur, the element present in the drug molecule but absent in that of the coformer (Figure 4d). As is evident by comparing parts c and d of Figure 4, the sulfur distribution is so uniform that the map accurately reproduces the sample morphology. This indicates that the sample is not a simple mixture of the two components but an interaction between them has occurred, leading to the formation of multicomponent crystals. This is a further evidence that the SEM-EDS technique is an important source of information in the study of multicomponent systems.^{17,19,23}

Parts b and c of Figure 5 show the solid-state ^{13}C CPMAS spectra of bumetanide and 4-aminobenzoic acid, respectively. The peak assignment was taken from the literature as concerns the acid,²⁴ whereas in the case of bumetanide it was derived by a direct comparison with the high-resolution liquid spectrum (see Figure 5a). With respect to the molecule in the liquid state, crystalline bumetanide shows a 6 ppm deshielding of the C=O (13), a 3–5 ppm deshielding of the aliphatic carbons (2–5), and smaller variations of the chemical shifts of the aromatic carbons 6, 7, 8, and 12. These findings call for the onset of a complex scheme of weak interactions when passing from the liquid to the solid state. However, in the absence of a detailed description of the crystal structure, which to our knowledge is not yet available in the literature, more information cannot be obtained within our simplified approach.

Figure 6 shows the ^{13}C CPMAS spectrum of the cocrystal *BAB:1kn*, together with those of the constituting molecules. We can easily appreciate the cocrystal formation, due to the substantial differences between its spectrum and the simple superposition of the spectra of the constituting molecules.²⁵ By inspecting the cocrystal spectrum in more detail, we observe that the peaks of carbons E and D of the acid are shifted upfield by about 3 ppm with respect to the pure compound, whereas carbons A, B, and C are practically unaffected. Concerning the bumetanide part, we observe some small effects of the carbons near the SO_2NH_2 group. Therefore, we can envisage an interaction between the amino group of the acid and the

SO_2NH_2 group of bumetanide (see also DFT model 4, Figure 13). Interestingly, the chemical shifts of both the C=O do not change upon the cocrystal formation. This result can be rationalized by inferring the onset of a carboxyl–carboxyl interaction (model 2, Figure 13) similar to those already taking place in the pure compounds. Finally, in the cocrystal, the bumetanide aliphatic carbon peaks are shifted upfield to the same positions observed on the pure molecule in solution. This calls for a disruption of the close packing expected in bumetanide crystal.

3.2. The Dry Grinding Product. The XRPD analysis puts into evidence that grinding promotes a gradual interaction between drug and coformer. After 15 min of grinding, the pattern (Figure 7a) shows the typical diffraction peaks of the

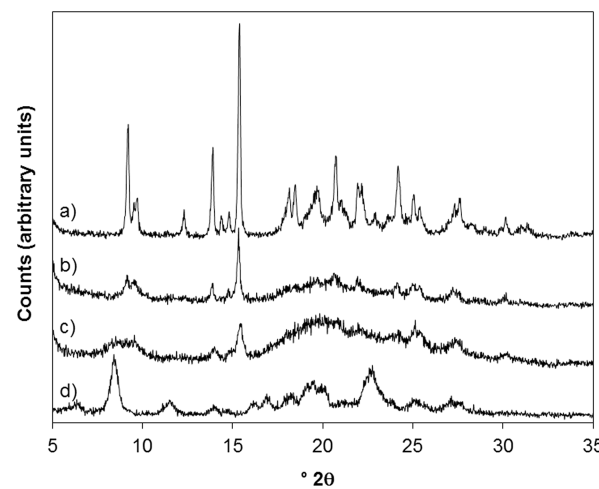


Figure 7. XRPD patterns of (a) *BAB1:1mp15min*, (b) *BAB1:1mp30min*, (c) *BAB1:1mp90min*, and (d) *BAB1:1mp120min*.

pure components. Upon longer grinding, the peak intensity decreases progressively, thus indicating that the crystalline powders are changing to amorphous phase(s) (Figure 7b and c). In the pattern of the sample *BAB1:1mp120min*, some new and broad peaks appear at positions different from those of the starting components, thus indicating a new phase (likely a cocrystal) formation (Figure 7d). Then, the pattern does not

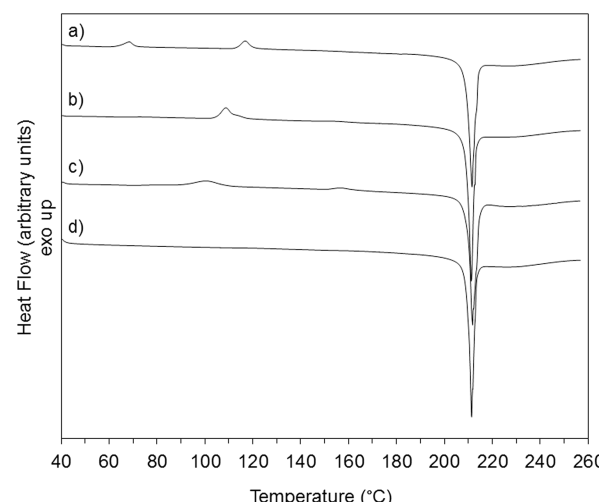


Figure 8. DSC curves of (a) *BAB1:1mp15min*, (b) *BAB1:1mp30min*, (c) *BAB1:1mp90min*, and (d) *BAB1:1mp120min*.

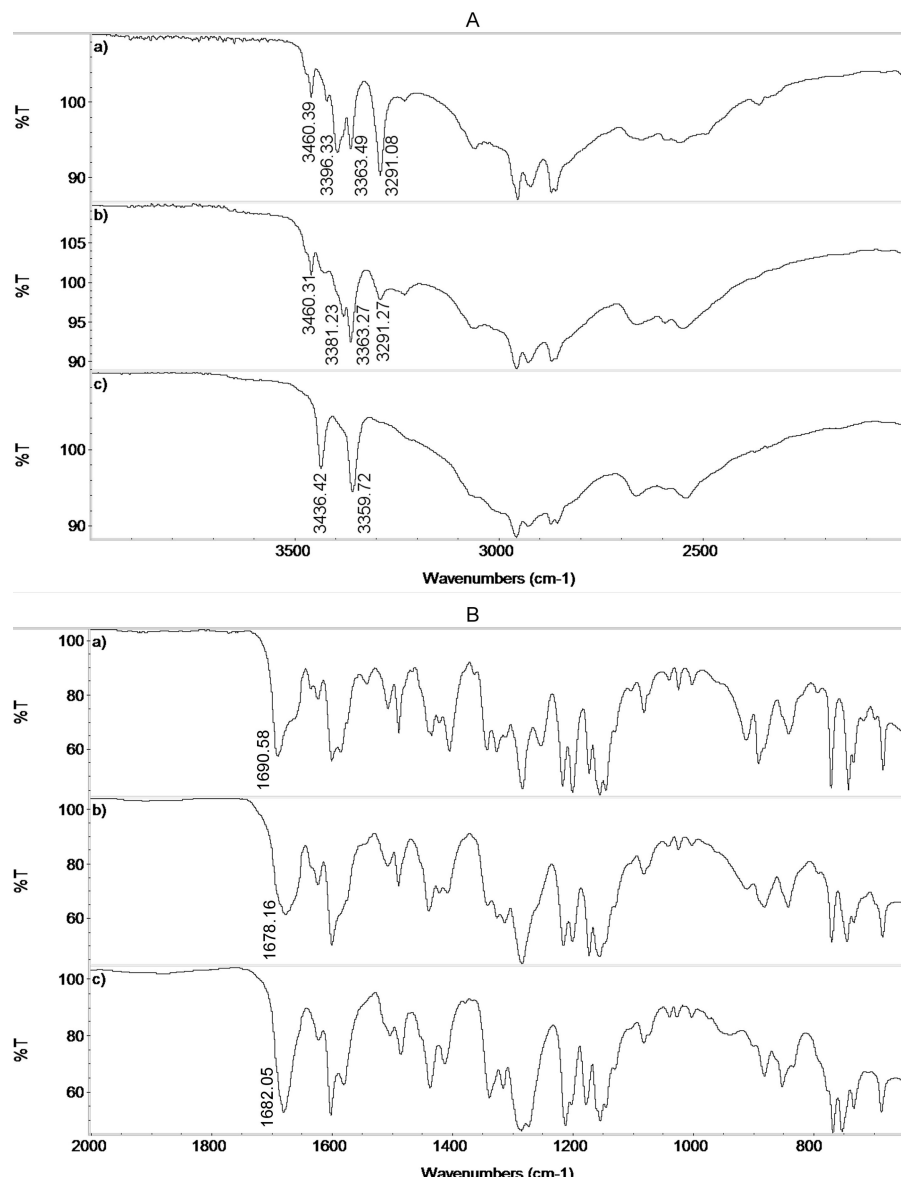


Figure 9. FT-IR spectra of (a) *BAB1:1mp15min*, (b) *BAB1:1mp90min*, and (c) *BAB1:1mp120min* in the frequency region 4000–2000 cm^{-1} (A) and 2000–650 cm^{-1} (B).

change any more even after 10 h of grinding (not shown). The diffraction peaks of the samples ground for at least 120 min fall at 2θ values different from those of the product obtained by kneading, suggesting that dry grinding leads to formation of a different cocrystal phase. The results put also into evidence that bumetanide–4-aminobenzoic acid cocrystallization, during dry grinding, proceeds via an amorphous intermediate. The amorphous phase subsequently transforms into the cocrystal one.

The DSC curve of the *BAB1:1mp15min* sample (Figure 8a) shows exothermic effects between 95 and 180 °C followed by a sharp melting peak at the same onset temperature, and with the same enthalpy change of the *BAB1:1kn* sample. The DSC curve changes with grinding in terms of temperature and area of the exothermal effects, as shown in Figure 8. The exothermic effects are not reversible, since, after a first heating to 185 °C and cooling to room temperature, they are no more present in a second scan. Since the XRPD pattern of the sample heated up to 185 °C is similar to that of the phase obtained by kneading, we can conclude that the exothermic effects lead to the

crystallization of a cocrystal with the same structure of the kneaded product.

In agreement with the XRPD analysis, also the FT-IR spectrum of the binary system changes with mechanical stress duration (Figure 9). In particular, in the spectrum of the *BAB1:1mp15min* sample (Figure 9a), all the vibrational features can be attributed to the starting components. On increasing grinding time, the spectral behavior shows increasing differences up to the *BAB1:1mp120min* sample (Figure 9c) and after that no more changes are observed. The main differences concern the absorption peaks of the sulfonamide and the carboxylic groups of bumetanide, the amino and the carboxylic groups of the coformer, i.e., the same functional groups involved in the interaction established in the *BAB1:1kn* sample. However, the spectra of ground and kneaded samples are not similar, confirming that two different solid phases have been formed. However, the FT-IR spectrum of all ground samples heated up to 185 °C (Figure 10) becomes similar to that of the kneaded sample, thus confirming that heating leads to the same

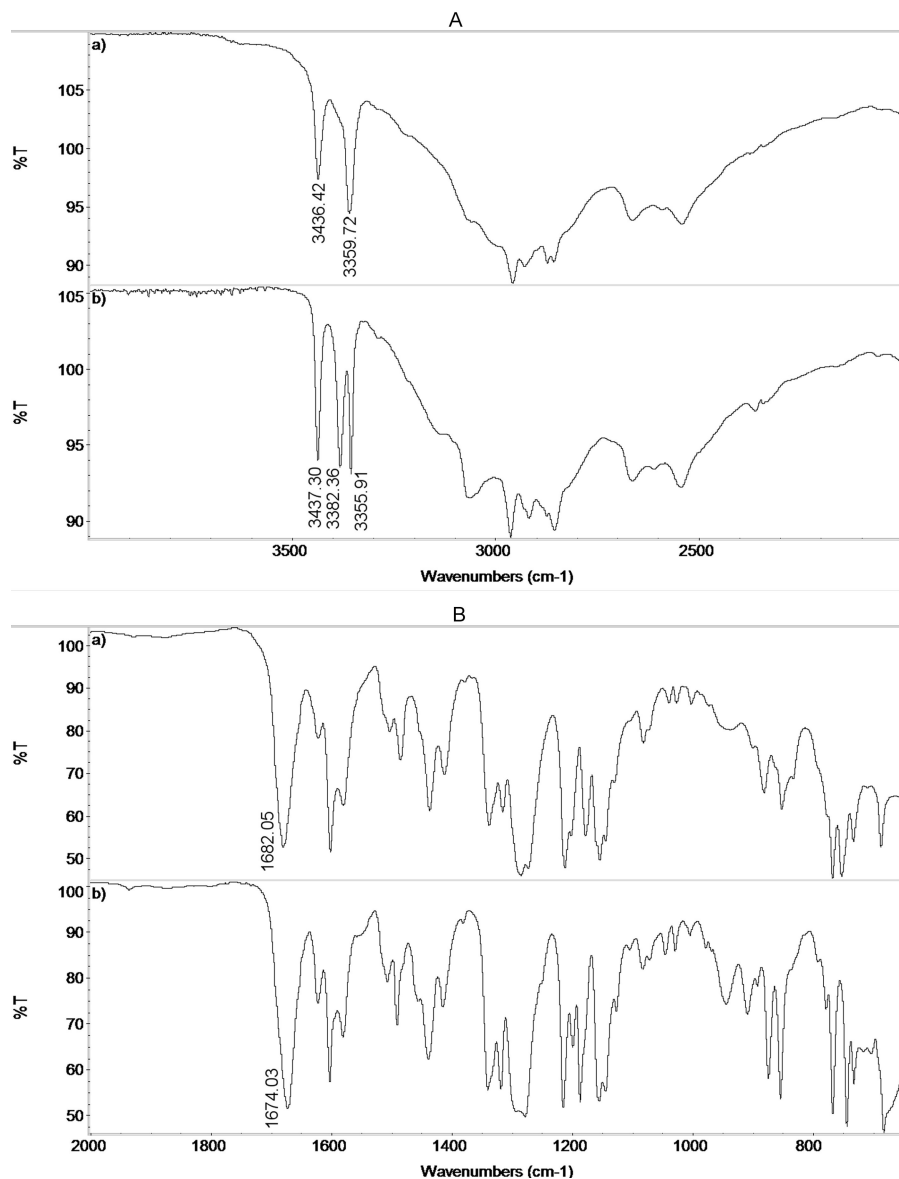


Figure 10. FT-IR spectra of (a) *BAB1:1mp120min* and (b) *BAB1:1mp120min* heated up to 185 °C in the frequency region 4000–2000 cm⁻¹ (A) and 2000–650 cm⁻¹ (B).

cocrystal obtained by wet grinding, in agreement with the XRPD measurements.

The SEM-EDS analysis supports the results obtained from X-ray diffraction and FT-IR spectroscopy. Comparing the SEM micrograph of the *BAB1:1mp15min* sample (Figure 11a) with the sulfur map (Figure 11b), the difference is evident: some particles present in the SEM image are missing in the sulfur map. Indeed, the XRPD has already proved that the cocrystal has not yet been formed after 15 min of grinding. In contrast, for the samples ground 120 min, the SEM image (Figure 11c) and the sulfur map (Figure 11d) are very similar, proving that a homogeneous compound was formed. In Figure 11e and f, the morphologic changes that occurred in the *BAB1:1mp15min* sample as a consequence of heating to 185 °C are evident. New aggregates of fine needles are present and little sticks are growing on the surface of the big particles, which likely must be attributed to the new cocrystal phase.

Figure 12 shows the ¹³C CPMAS spectrum of *BAB1:1mp120min* together with those of the constituting molecules.

Again, we are fully confident on the formation of a cocrystal, but the analysis of its spectrum is even more complex than in the previous case. In this case, we observed a shift downfield of acid carbon D and bumetanide carbon 6. Interestingly, carbon E of the acid is shifted upfield, in contrast to what happens for cocrystal *BAB1:1kn*. Finally, shifts upfield are observed for carbons 15, 16, and 17 of bumetanide.

3.3. Modeling H-Bonding Interactions by DFT Calculations. With the aim of modeling the H-bonding interactions within the cocrystals, we have located six different complexes between bumetanide and 4-aminobenzoic acid by DFT calculations at the B3LYP/6-31+G(d,p) level of theory, in the gas phase. In order to simulate frequencies of the vibrational modes characterizing the moieties involved in H-bonding, we computed frequency calculations at the same level of theory, in the approximation of the harmonic oscillator. The structures of the complexes (Figure 13) geometrically describe the interactions between the carboxyl and amino moieties of the aminobenzoic acid (**1–3** and **4–6**, respectively), and the three

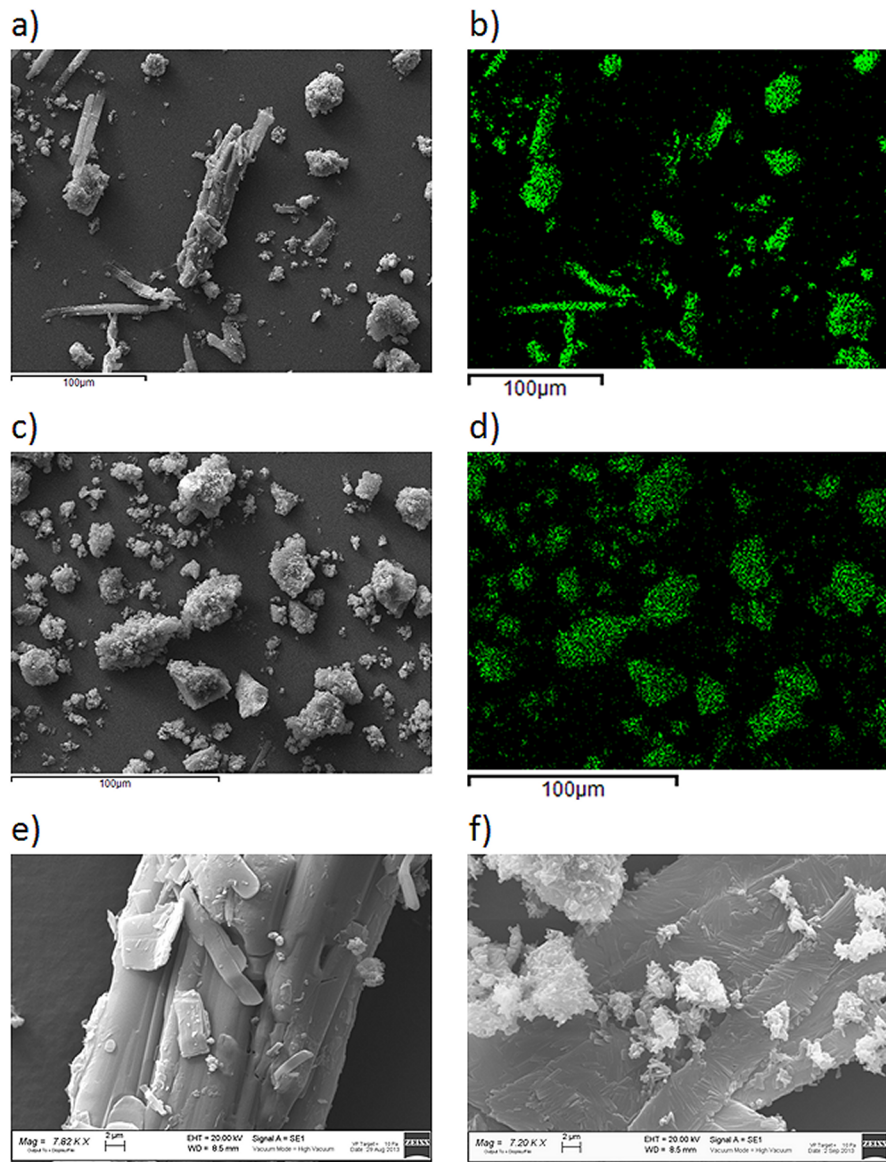


Figure 11. Microphotographs of (a) *BAB1:1mp15min*, (c) *BAB1:1mp120min*, (e) *BAB1:1mp15min* at high magnification, (f) *BAB1:1mp15min* heated up to 185 °C, and (b, d) the sulfur maps of, respectively, *BAB1:1mp15min* and *BAB1:1mp120min*.

functional groups embedded into bumetanide. For clarity, only the most stable conformers for each combination of interacting functional groups have been reported in Figure 13.

The most stable complex is **2**, thanks to a strong H-bonding interaction between the carboxyl groups, which exhibit COO-H stretching mode frequencies at 3147 and 2900 cm⁻¹ for 4-aminobenzoic acid and bumetanide, respectively. Complex **1** is less stable than **2** only by 4.6 kcal/mol, due to a less effective H-bonding involving the carboxyl and sulfamide moieties, as inferred by higher COO-H and C=O stretching mode frequencies (3433 vs 3147 cm⁻¹ and 1724 vs 1682 cm⁻¹). A more comprehensive list of the stretching mode frequencies characterizing the functional groups involved in the H-bonding has been reported in Table 1.

We also optimized the geometries and energies of the three complexes characterizing the H-bonding interactions of the dimer of bumetanide (**7–9**, Figure 14), at the very same level of theory, since no experimental data are available on the crystallographic structure of bumetanide. The stability order

follows a trend similar to that observed for bumetanide and 4-aminobenzoic acid, with the dimer complex involving both of the carboxyl moieties (**8**) which is slightly more stable than **7** (by 3.8 kcal/mol), where the carboxyl group interacts with the sulfonamide. This finding is in agreement with the NMR results (see Figure 5a,b).

The regular repetition in space of sulfonamide and carboxyl interacting groups, which maximizes the H-bonding in a crystal structure, should be achieved for bumetanide through complex **7**. On the contrary, the periodicity of the bumetanide–4-aminobenzoic acid cocrystals may be described by two distinctive models with comparable energy: (i) the first one resulting from the combination of complexes **2** and **4**; (ii) the second one coupling the H-bonding complex **1** with **5**. The first model results are only 3.1 kcal/mol more stable than the second model results. This finding is in good agreement with the NMR results reported in Figure 6. This dual model may also rationalize the differences in the IR absorptions experimentally measured for the sulfonamide and the carboxylic

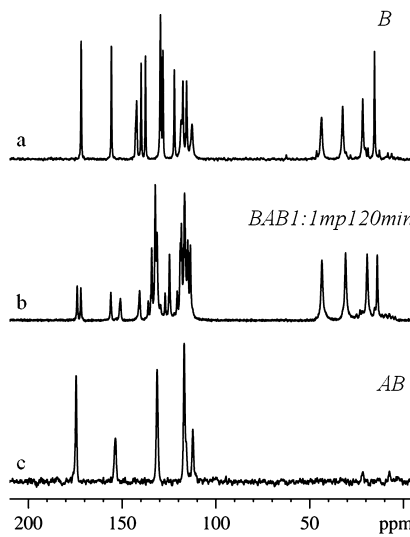


Figure 12. ^{13}C CPMAS NMR spectra of (a) bumetanide polycrystalline sample, (b) BAB1:Imp120min cocrystal, and (c) 4-aminobenzoic acid.

groups of bumetanide, and the amino and carboxylic groups of the coformer, also accounting for the two polymorph cocrystals detected.

3.4. Solubility and Dissolution Rate. The experimental value of bumetanide water solubility at 21°C is very low ($23.3 \pm 2.3 \text{ mg/L}$) (see Figure 15) and in agreement with the value reported in the literature of 26 mg/L ,²⁶ but the

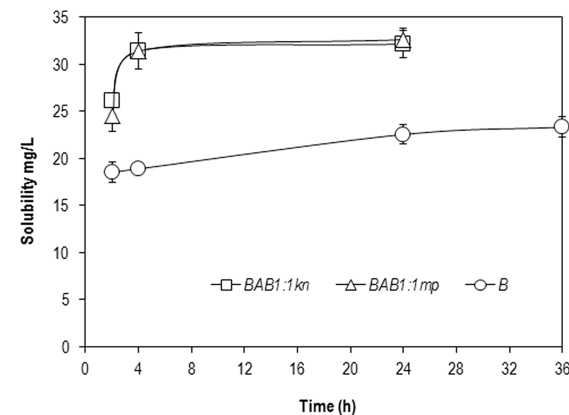


Figure 15. Water solubility at 21°C of bumetanide (B) and of the new samples BAB1:1kn and BAB1:Imp120min .

equilibrium solubility is reached very slowly in almost 36 h. With the same conditions, the new samples BAB1:1kn and BAB1:Imp120min showed improved solubility of 32.2 ± 1.4 and $32.6 \pm 1.2 \text{ mg/L}$, respectively, and this enhancement could prevent saturation of the biologic fluids during the dissolution/absorption process. Moreover, the value at equilibrium is reached quite quickly compared to the drug alone, in about 4 h. Neither the drug nor the coformer reprecipitated during the following 24 h. A very fast dissolution rate could be a great advantage from a pharmaceutical point of view, because the drug should dissolve very quickly after oral administration, to obtain the whole dose available for absorption in short times.

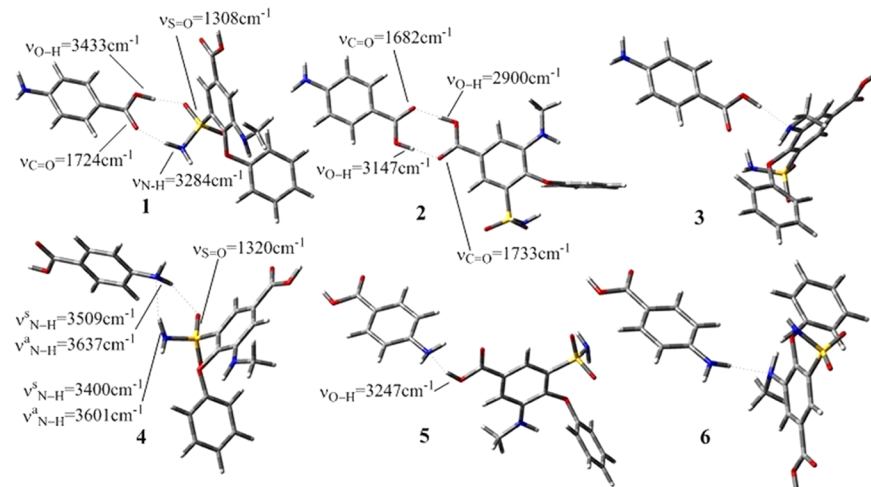


Figure 13. Geometries of the H-bonded complexes between bumetanide and 4-aminobenzoic acid, optimized by DFT calculations at the B3LYP/6-31+G(d,p) level, in the gas phase, together with the main vibrational frequencies in cm^{-1} .

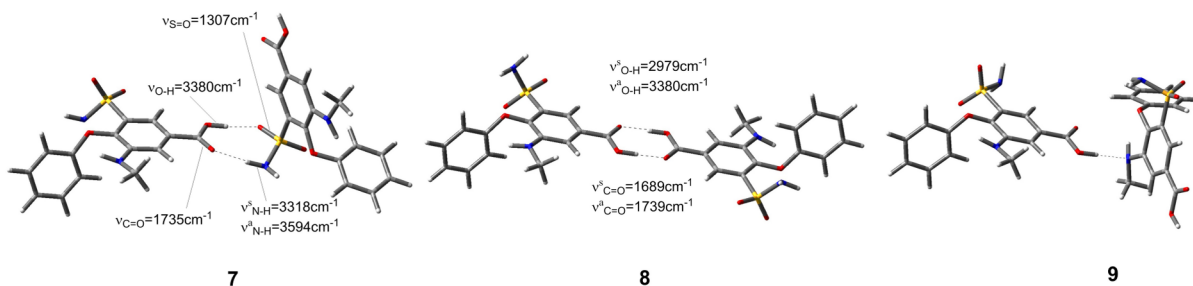


Figure 14. Geometries of H-bonded complexes describing the bumetanide, optimized by DFT calculations at the B3LYP/6-31+G(d,p) level, in the gas phase, together with the main vibrational frequencies, in cm^{-1} .

Table 1. Vibrational Frequencies of the Stretching Modes of the Functional Groups Involved in the H-Bonding within the Most Stable Complexes between Bumetanide and 4-Aminobenzoic Acid (1, 2, 4, 5), and Bumetanide (7, 8) Modelled by DFT Calculations at the B3LYP/6-31+G(d,p) Level, in the Gas Phase, Assuming the Approximation of the Harmonic Oscillators^a

Moieties	Vibrational mode	Stretching frequencies in the complexes /cm ⁻¹					
		1	2	4	5	7	8
 Bumetanide	C=O	1797	1733	1777	1784	1735	1689 (symm.)
	O-H	3768	2899	3766	3247	1798	1739 (asymm.)
	S=O (asymm.)	1308	1332	1320	1332	3380	2979 (symm.)
	N-H (symm.)	3284	3510	3400	3510	3367	3090 (asymm.)
	N-H (asymm.)	3592	3633	3601	3633	1307	1319
 4-Aminobenzoic acid	C=O	1724	1682	1777	1784	-	-
	N-H	3593	3597	3509	3491	-	-
		3707	3711	3637	3615	-	-

^aThe relative stability of the remaining complexes 3–6 follows the order: 2 > 1 > 5 > 4 ≥ 3 > 6 (Table 2).

Table 2. Relative Stability of the Remaining Complexes 1–6 and 7–9 in kcal/mol Computed at the B3LYP/6-31+G(d,p) Level of Theory in the Gas Phase

ΔE (kcal/mol), bumetanide–4-aminobenzoic acid									ΔE (kcal/mol), bumetanide
1	2	3	4	5	6	7	8	9	
4.6	0.0	10.6	10.5	8.8	15.1	3.8	0.0	10.9	

4. CONCLUSIONS

Here we reported the mechanochemical synthesis of bumetanide–4-aminobenzoic acid molecular cocrystals. Both wet (kneading) and dry grinding proved to be low-cost, easy, efficient, and green approaches for obtaining cocrystals. Two different polymorphs of cocrystal in the same stoichiometric ratio (1:1) were obtained. However, the phase obtained by dry grinding is metastable and does change to the same polymorph obtained by kneading (i.e., the stable one) on heating at 185 °C.

The combined use of spectroscopy and DFT calculations demonstrates that both polymorphs are molecular cocrystals sustained by a complex motif of H-bonding interactions. More in detail, the periodicity of the bumetanide–4-aminobenzoic acid cocrystals may be described by the combination of two complexes involving carbonyl–carbonyl and amino–sulfonamide group interactions, respectively.

The cocrystals showed a clear enhancement in water solubility and a faster dissolution rate compared to the drug alone. These improved physicochemical properties could guarantee a better drug formulation in low-volume parenteral dosage forms and, in the case of oral administration, may improve drug availability for a faster and complete *in vivo* absorption.

AUTHOR INFORMATION

Corresponding Author

*Phone: +39 0382 987667. E-mail: giovanna.bruni@unipv.it

Notes

The authors declare no competing financial interest.

REFERENCES

- (1) Steed, J. W. *Trends Pharmacol. Sci.* **2013**, *34*, 185–193.
- (2) Sun, C. C. *Expert Opin. Drug Delivery* **2013**, *10*, 201–213.
- (3) FDA. *Guidance for Industry: Regulatory Classification of Pharmaceutical Co-crystals*, 2013.
- (4) Ter Horst, J. H.; Cains, P. W. Co-crystal polymorphs from a solvent-mediated transformation. *Cryst. Growth Des.* **2008**, *8*, 2537–2542.
- (5) Chun, N. H.; Wang, I. C.; Lee, M. J.; Jung, Y. T.; Lee, S.; Kim, W. S.; Choi, G. J. Characteristics of indomethacin–saccharin (IMC–SAC) co-crystals prepared by an anti-solvent crystallization process. *Eur. J. Pharm. Biopharm.* **2013**, *85*, 854–861.
- (6) Padrela, L.; Rodrigues, M. A.; Velaga, S. P.; Matos, H. A.; De Azevedo, E. G. Formation of indomethacin–saccharin cocrystals using supercritical fluid technology. *Eur. J. Pharm. Sci.* **2009**, *38*, 9–17.
- (7) Dhumal, R. S.; Biradar, S. V.; Paradkar, A. R.; York, P. Particle engineering using sonocrystallization: salbutamol sulphate for pulmonary delivery. *Int. J. Pharm.* **2009**, *368*, 129–137.
- (8) Braga, D.; Maini, L.; Grepioni, F. Mechanochemical preparation of co-crystals. *Chem. Soc. Rev.* **2013**, *42*, 7638–7648.
- (9) Friscic, T.; Childs, S. L.; Rizvi, S. A. A.; Jones, W. The role of solvent in mechanochemical and sonochemical cocrystal formation: a solubility-based approach for predicting cocrystallisation outcome. *CrystEngComm* **2009**, *11*, 418–426.
- (10) Weyna, D. R.; Shattock, T.; Vishweshwar, P.; Zaworotko, M. Synthesis and structural characterization of cocrystals and pharmaceutical cocrystals: mechanochemistry vs slow evaporation from solution. *Cryst. Growth Des.* **2009**, *9*, 1106–1123.
- (11) Delori, A.; Friscic, T.; Jones, W. The role of mechanochemistry and supramolecular design in the development of pharmaceutical materials. *CrystEngComm* **2012**, *14*, 2350–2362.
- (12) Asbury, M. J.; Gatenby, P. B. B.; O’Sullivan, S.; Bourke, E. Bumetanide: Potent New “Loop” Diuretic. *Br. Med. J.* **1972**, *1*, 211–213.
- (13) Lau, H. S. H.; Hyneck, M. L.; Berardi, R. R.; Swartz, R. D.; Smith, D. E. Kinetics, dynamics, and bioavailability of bumetanide in healthy subjects and patients with chronic renal failure. *Clin. Pharmacol. Ther.* **1986**, *39*, 635–645.
- (14) Ward, A.; Heel, R. C. Bumetanide. A review of its pharmacodynamic and pharmacokinetic properties and therapeutic use. *Drugs* **1984**, *28*, 426–464.
- (15) Serajuddin, A. T. M. Salt formation to improve drug solubility. *Adv. Drug Delivery Rev.* **2007**, *59*, 603–616.
- (16) Winston, O.; Cheung, E. Y.; Schultz, K. A.; Smith, C.; Bourassa, J.; Hickey, M. B. Sodium and potassium salts of bumetanide trihydrate: Impact of counterion on structure, aqueous solubility and dehydration kinetics. *CrystEngComm* **2012**, *14*, 2428–2434.
- (17) Bruni, G.; Maietta, M.; Berbenni, V.; Bini, M.; Ferrari, S.; Capponi, D.; Boiocchi, M.; Milanese, C.; Marini, A. Preparation and characterization of carprofen co-crystals. *CrystEngComm* **2012**, *14*, 435–445.

- (18) Bruni, G.; Maietta, M.; Maggi, L.; Mustarelli, P.; Ferrara, C.; Berbenni, V.; Freccero, M.; Scotti, F.; Milanese, C.; Girella, A.; Marini, A. An Experimental and Theoretical Investigation of Loperamide Hydrochloride-Glutaric Acid Cocrystals. *J. Phys. Chem. B* **2013**, *117*, 8113–8121.
- (19) Bruni, G.; Maietta, M.; Maggi, L.; Mustarelli, P.; Ferrara, C.; Berbenni, V.; Milanese, C.; Girella, A.; Marini, A. Preparation and physico-chemical characterization of acyclovir co-crystals with improved dissolution properties. *J. Pharm. Sci.* **2013**, *102*, 4079–4095.
- (20) Borka, L. The polymorphism of bumetanide, of glibornuride and of chlorpromazine picrate. *Acta Pharm. Suec.* **1977**, *14*, 205–209.
- (21) Kuhnert-Brandstaetter, M.; Wurian, I.; Geller, M. Thermoanalytical and IR-spectroscopic studies on enantiotropic polymorphs of drugs. *Sci. Pharm.* **1982**, *50*, 3–11.
- (22) Schultheiss, N.; Newman, A. Pharmaceutical cocrystals and their physicochemical properties. *Cryst. Growth Des.* **2009**, *9*, 2950–2967.
- (23) Bruni, G.; Maietta, M.; Maggi, L.; Bini, M.; Capsoni, D.; Ferrari, S.; Boiocchi, M.; Berbenni, V.; Milanese, C.; Marini, A. Perphenazine-fumaric acid salts with improved solubility: preparation, physico-chemical characterization and in vitro dissolution. *CrystEngComm.* **2012**, *14*, 6035–6044.
- (24) Samsonowicz, M.; Hrynaszkiewicz, T.; Swisłocka, R. S.; Regulska, E.; Lewandowski, W. Experimental and theoretical IR, Raman, NMR spectra of 2-, 3- and 4-aminobenzoic acids. *J. Mol. Struct.* **2005**, *744–747*, 345–352.
- (25) Vogt, F. G.; Clawson, J. S.; Strohmeier, M.; Edwards, A. J.; Pham, T. N.; Watson, S. A. Solid state NMR analysis of organic cocrystals and complexes. *Cryst. Growth Des.* **2009**, *9*, 921–937.
- (26) <http://www.hmdb.ca/metabolites/HMDB15024>, Human Metabolome Database, version 3.5, Bumetanide, HMDB15024, accessed Dec 17, 2013.